

# Cardiomyocytes derived from human embryonic stem cells in pro-survival factors enhance function of infarcted rat hearts

Michael A Laflamme<sup>1,2,6</sup>, Kent Y Chen<sup>1-3,6</sup>, Anna V Naumova<sup>1,4</sup>, Veronica Muskheli<sup>1,2</sup>, James A Fugate<sup>1,2</sup>, Sarah K Dupras<sup>1,2</sup>, Hans Reinecke<sup>1,2</sup>, Chunhui Xu<sup>5</sup>, Mohammad Hassanipour<sup>5</sup>, Shailaja Police<sup>5</sup>, Chris O'Sullivan<sup>5</sup>, Lila Collins<sup>5</sup>, Yinhong Chen<sup>5</sup>, Elina Minami<sup>1,3</sup>, Edward A Gill<sup>3</sup>, Shuichi Ueno<sup>1,2</sup>, Chun Yuan<sup>1,4</sup>, Joseph Gold<sup>5</sup> & Charles E Murry<sup>1,2</sup>

**Cardiomyocytes derived from human embryonic stem (hES) cells potentially offer large numbers of cells to facilitate repair of the infarcted heart. However, this approach has been limited by inefficient differentiation of hES cells into cardiomyocytes, insufficient purity of cardiomyocyte preparations and poor survival of hES cell-derived myocytes after transplantation. Seeking to overcome these challenges, we generated highly purified human cardiomyocytes using a readily scalable system for directed differentiation that relies on activin A and BMP4. We then identified a cocktail of pro-survival factors that limits cardiomyocyte death after transplantation. These techniques enabled consistent formation of myocardial grafts in the infarcted rat heart. The engrafted human myocardium attenuated ventricular dilation and preserved regional and global contractile function after myocardial infarction compared with controls receiving noncardiac hES cell derivatives or vehicle. The ability of hES cell-derived cardiomyocytes to partially remuscularize myocardial infarcts and attenuate heart failure encourages their study under conditions that closely match human disease.**

The heart is one of the least regenerative organs in the body and, consequently, loss of myocardium to infarction or other diseases often leads to heart failure<sup>1-4</sup>. Stem cells offer the possibility of repairing damaged organs like the heart from their component parts, and there is an intensive effort to develop stem cell-based strategies for cardiac repair. Both adult and embryonic stem cells are being studied in preclinical models, and at least four types of autologous cells (skeletal myoblasts, bone marrow mononuclear cells, mesenchymal stem cells and endothelial progenitor cells) are being tested in early-stage clinical trials<sup>5-7</sup>. hES cells are an attractive population for cardiac repair because they can be isolated and maintained by well-established protocols, can be greatly expanded in culture and can be differentiated into definitive cardiomyocytes<sup>8-10</sup>. In addition, hES cell-derived cardiomyocytes have robust proliferative capacity both *in vitro*<sup>8,11,12</sup> and after implantation<sup>13</sup>, implying that delivery of an initially sub-therapeutic cell dose may suffice to obtain a functionally meaningful cardiac implant over time.

Initial studies with hES cell-derived cardiomyocytes have shown their capacity to form new myocardium in the uninjured heart<sup>13-15</sup>. One encouraging feature of these cells is that they appear capable of achieving at least some degree of electrical integration with surrounding host myocardium in such models<sup>14,15</sup>, unlike skeletal myoblast

grafts, which appear to remain electrically insulated<sup>16,17</sup>. To date, no studies have explored the suitability of hES cells for heart repair in the setting of myocardial infarction. Mechanical repair of the left ventricle represents a considerable therapeutic challenge, as it may require  $\sim 10^3$  times more cells to repopulate a human infarct than to form a pacemaker. For infarct repair with hES cell-derived cardiomyocytes to be feasible, it will be necessary to have a clinically scalable system to efficiently direct cardiomyocyte differentiation. Additionally, it will be necessary to ensure that the grafted cardiomyocytes survive to form enough new myocardium to replace the tissue lost to infarction, and to prevent immune rejection of the allogeneic cells.

## RESULTS

### Embryoid body-derived transplants: poor engraftment and purity

Previously we demonstrated that embryoid body-derived human cardiomyocytes form stable myocardial grafts when directly injected into the uninjured hearts of athymic (nude) rats<sup>13</sup>. We also showed that the size of grafts in the normal heart could be increased fourfold by prior heat-shock treatment of the cells<sup>13</sup>. We therefore tested the ability of  $5 \times 10^6$  heat-shocked human cardiomyocytes to form stable grafts in nude rat heart that had been infarcted by permanent coronary artery ligation. In contrast to our 90% engraftment success rate in the

<sup>1</sup>Center for Cardiovascular Biology, Institute for Stem Cell and Regenerative Medicine, <sup>2</sup>Department of Pathology, University of Washington, 815 Mercer Street, Seattle, Washington 98109, USA. <sup>3</sup>Department of Medicine/Cardiology, University of Washington, 1959 NE Pacific Street, Seattle, Washington 98195, USA. <sup>4</sup>Vascular Imaging Laboratory, Department of Radiology, University of Washington, 815 Mercer Street, Seattle, Washington 98109, USA. <sup>5</sup>Geron Corporation, 230 Constitution Drive, Menlo Park, California 94025, USA. <sup>6</sup>These authors contributed equally to this work. Correspondence should be addressed to C.E.M. (murry@u.washington.edu).

Received 8 May; accepted 13 July; published online 26 August 2007; doi:10.1038/nbt1327

uninjured heart, only 6 of 34 infarcts (18%) contained any human myocardial grafts (as determined by *in situ* hybridization with a human-specific pan-centromeric probe<sup>18</sup>; approximately ten vibratome sections per heart). Furthermore, these grafts were generally much smaller than those observed in the normal heart, often consisting of small clusters of a few cells. Of concern, even in the six hearts that did contain surviving human graft, all grafts included a substantial component of noncardiac elements, including rare epithelium-lined cysts (Supplementary Fig. 1 online). This finding stands in stark contrast to our previous experience with grafting into uninjured hearts, where noncardiac elements were efficiently cleared over time<sup>13</sup>. These experiments indicated the need to use a system with greater cardiomyocyte yield and purity than our embryoid body with serum-induction model. They also clearly demonstrated that death of grafted cardiomyocytes was a much bigger problem in the infarct than in the noninfarcted heart.

### Directed cardiac differentiation of hES cells

To enhance the yield and purity of cardiomyocytes from hES cells, we used a recently developed technique to direct the differentiation of hES cells into cardiomyocytes by sequential treatment of high-density undifferentiated monolayer cultures with activin A and bone morphogenetic protein 4 (BMP4). In contrast to our previous embryoid body-based system, which used serum to induce differentiation (typically yielding <1% cardiomyocytes), the activin/BMP protocol consistently yielded >30% cardiomyocytes. After a simple Percoll gradient centrifugation step, cultures of  $82.6 \pm 6.6\%$  cardiomyocytes (range 71–95%) were readily obtained (Supplementary Fig. 2 online).

Some calculations indicate the potential scalability of this directed cardiac differentiation protocol. For the grafting experiments using this cell population ( $n = 4$  preparations) described below, we initially seeded  $3.9 \pm 0.8 \times 10^7$  (range  $(2.4\text{--}5.8) \times 10^7$ ) undifferentiated H7 hES cells. After directed differentiation and harvesting by enzymatic dispersion, these cultures generated a total differentiated cell yield of  $2.3 \pm 1.0 \times 10^8$  cells. These differentiated cells then underwent Percoll gradient centrifugation, and  $69 \pm 10\%$  of the total cell population was recovered from the cardiomyocyte-enriched fractions. This corresponded to a Percoll-enriched cell yield of  $1.3 \pm 0.3 \times 10^8$  (range  $0.7 \pm 2.0 \times 10^8$ ). Taking into account the resultant mean cardiac

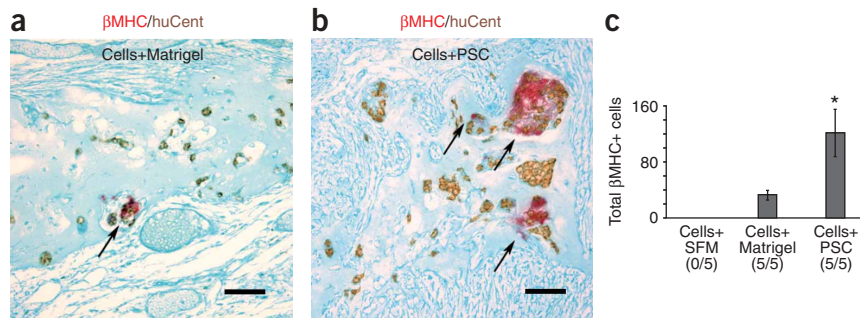
purity of 82.6%, we calculated that each starting undifferentiated hES cell generated approximately three human cardiomyocytes.

### Prosurvival cocktail improves graft survival in infarcted hearts

The poor engraftment rate in the infarcted heart suggested that most of our hES cell-derived cardiomyocytes were dying. We hypothesized that graft cell injury was initiated by three principal pathways: ischemia, due to the absence of a vasculature within the injected cell clumps and their delivery into an ischemic environment; anoikis, due to the need to detach these anchorage-dependent cells from their substrate for injection; and inflammation-related factors, such as free radicals, cytokines and natural killer cells. We carried out a series of histology based experiments to identify which of these initiators and their downstream effectors were causing the cell death. None of the following modifications resulted in improved engraftment: (i) induction of infarcts by 60 min of ischemia followed by reperfusion, to reduce the severity of ischemia in the infarct zone, (ii) overexpression of the antiapoptotic proteins Bcl-2 and Akt in graft cells by adenoviral transduction before transplantation (using two different multiplicities of infection), (iii) delivery of the prosurvival growth factor, insulin-like growth factor 1 (IGF-1), in a Pluronic gel directly injected with the cells, (iv) use of allopurinol plus uricase<sup>19</sup> in an attempt to block production of the 'danger signal', uric acid, from dead or dying cells, (v) depletion of natural killer cells from the athymic rats using an anti-asialo-GM1 antibody, (vi) use of a broad-spectrum immunosuppressive and anti-inflammatory cocktail that included dexamethasone, ibuprofen, complement-depleting cobra-venom factor and anti-asialo-GM1. In all of these experiments, echocardiographic analysis consistently showed that the resulting tiny human cardiac grafts did not attenuate postinfarct ventricular dilation or enhance fractional shortening compared with control infarcted hearts.

These results suggested that multiple, parallel processes were contributing to graft cell death, and that blocking one pathway simply led to cell death by another. This prompted us to develop a multi-component, prosurvival cocktail (PSC) targeting key points of potential death pathways. The PSC included Matrigel to prevent anoikis<sup>20</sup>, a cell-permeant peptide from Bcl-XL to block mitochondrial death pathways<sup>21</sup>, cyclosporine A to attenuate cyclophilin D-dependent mitochondrial pathways<sup>22,23</sup>, a compound that opens ATP-dependent

**Figure 1** Protection of hES cell-derived cardiomyocyte grafts by the pro-survival cocktail. (a,b) Histologic analysis of graft cell survival. Heat-shocked hES cell-derived cardiomyocytes were injected into infarcted hearts of nude rats in the presence of SFM, Matrigel-only (a, Cells+Matrigel), or the full pro-survival cocktail (PSC) including Matrigel (b, Cells+PSC) ( $n = 5$  per group). Sections were stained with an antibody to  $\beta$ -myosin heavy chain ( $\beta$ MHC, red chromagen) as well as a human-specific pan-centromeric *in situ* hybridization probe (huCent, brown DAB deposit) to identify total human (that is, huCent+) and specifically human cardiac (that is,  $\beta$ MHC and huCent double-positive) graft cells. The human cardiomyocytes, indicated by arrows, were significantly more abundant in histologic sections from the Cells+PSC group than in Cells+Matrigel alone group. Histology is not depicted from the recipients of cells in SFM alone because none of these hearts showed even a single surviving human nucleus after 1 week. Counterstain, fast green; scale bar, 50  $\mu$ m. (c) Quantification of hES cell-derived cardiomyocyte graft size. Although no grafts were detected in any rats receiving hES cell-derived cardiomyocytes delivered in SFM alone (Cells+SFM), all rats receiving cells delivered in Matrigel-only (Cells+Matrigel) or in the full prosurvival cocktail (Cells+PSC) showed surviving graft (5/5 rats per group). However, recipients of cells in the full prosurvival cocktail (Cells+PSC) showed a mean of approximately fourfold more  $\beta$ -myosin-positive graft cells than did the Matrigel-only group. Note that counts indicate the total number of cells observed on sampled sections, not the total number of cells per heart. \*,  $P < 0.05$ .



K<sup>+</sup> channels (pinacidil) to mimic ischemic preconditioning<sup>24</sup>, IGF-1 to activate Akt pathways<sup>25</sup> and the caspase inhibitor ZVAD-fmk<sup>26</sup>. To test this regimen, we induced myocardial infarcts by 60 min of ischemia followed by reperfusion, and cardiomyocytes were transplanted at 4 d postinfarction, when angiogenesis associated with wound repair was at its maximum in this model and survival of grafted rat cardiomyocytes is the longest<sup>27</sup>. We first studied graft size by histology 1 week after transplantation, comparing results from cardiomyocytes treated with heat shock only (delivered in serum-free medium (SFM)), heat shock plus Matrigel or heat shock plus PSC (Fig. 1). Consistent with previous experience, none of the five reperfused infarcts in the heat shock-only group had detectable grafts. In contrast, 100% of infarcts receiving cardiomyocytes treated with heat shock and Matrigel had detectable grafts. Furthermore, in hearts receiving cardiomyocytes delivered with PSC, human myocardial graft size was fourfold larger than in those treated with heat shock plus Matrigel, indicating substantially improved engraftment resulting from additional factors in the cocktail. Although even these grafts were quite small at the 1-week time point examined, in previous studies of uninjured hearts we observed a sevenfold increase in graft size between 1 and 4 weeks after implantation, suggesting that we could obtain much larger grafts at later time points.

### Partial remuscularization of the infarct

We next performed 4-week studies to assess the long-term consequences of engraftment on infarct structure and function. Infarcts were induced by 60 min of ischemia followed by reperfusion. Rats were studied by echocardiography 2 d later to establish a pretreatment baseline. To stratify animals into groups with comparable infarct severities, we excluded from the study rats with a baseline fractional shortening >40% or subsequently shown to have no histologically identifiable infarct. Four days postinfarction (2 d after the baseline echocardiography), we transplanted  $10 \times 10^6$  direct-differentiated hES cell-derived cardiomyocytes into the infarcted region using heat shock and the PSC protocol. Control rats received injections into the infarct of PSC without cells, SFM without cells or PSC plus noncardiac cells (derived by differentiating hES cells in the absence of activin A or BMP4). At 4 weeks postengraftment, rat heart function was assessed again by echocardiography and magnetic resonance imaging (MRI) was performed to provide high-resolution analysis of cardiac structure and function. The rats were killed, and their hearts were harvested to determine infarct size and the size, distribution and composition of grafts. Picrosirius red histochemical staining was used to define the boundaries of the infarct zone, and subsequent histomorphometry indicated that infarct size did not differ among the three groups, averaging  $10.6 \pm 1.3\%$  of the left ventricle in PSC plus heat-shocked cardiomyocytes,  $9.2 \pm 0.7\%$  in hearts receiving PSC only,  $10.6 \pm 0.8\%$  in hearts receiving SFM-only and  $11.2 \pm 1.5\%$  in hearts receiving noncardiac cells.

In contrast to our previous experiments using single anti-death interventions, all of the hearts that received cardiomyocytes in the heat shock-plus-PSC group showed hES cell-derived cardiac implants after 4 weeks, and, in some cases, the grafts had remuscularized a significant portion of the infarct zone (Fig. 2). The human myocardium was readily visualized by its expected, strong expression of  $\beta$ -myosin heavy chain (Fig. 2a–h). As expected, the  $\alpha$ -myosin heavy chain-expressing rat myocardium was labeled by the SMHC antibody (which recognizes both  $\alpha$ - and  $\beta$ -myosin heavy chain) but not the  $\beta$ -myosin heavy chain-specific antibody (Fig. 2e). Additionally, all  $\beta$ -myosin-positive cells also stained with a human-specific pan-centromeric *in situ* probe (Fig. 2a–b, 2d), whereas the surrounding rat cells were uniformly

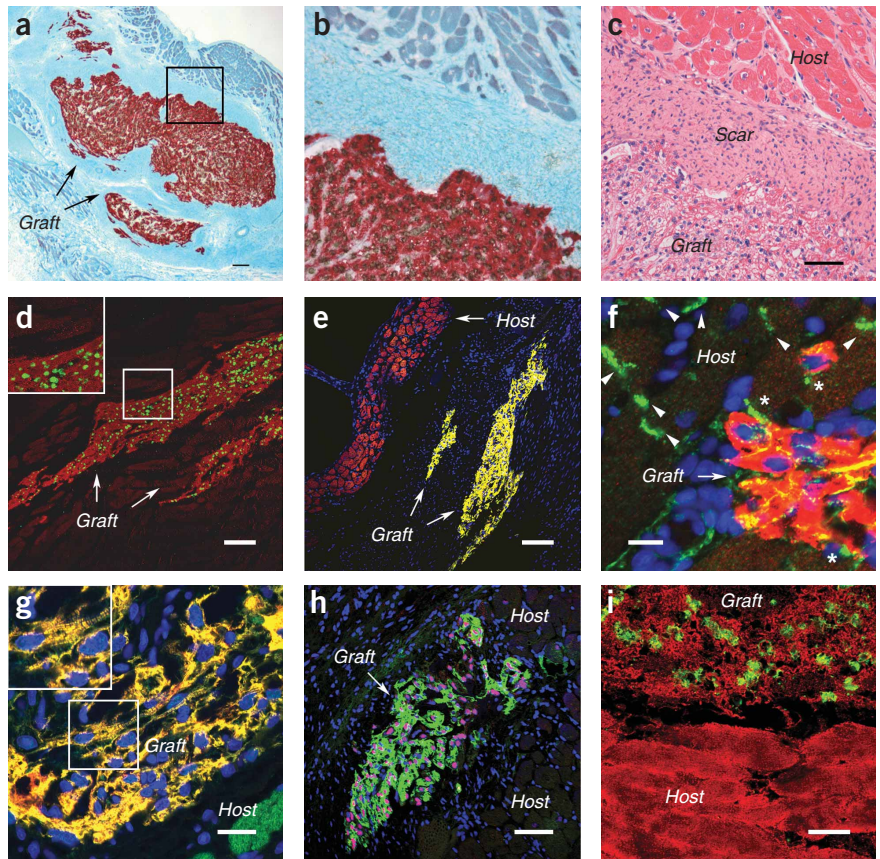
negative for this probe. Human myocardial graft size averaged  $4.1 \pm 0.9\%$  of the infarct, with a maximum size of 10.7% of the infarct. Although some of the human myocardium was located within the peri-infarct (border) zone, the vast majority ( $88.6 \pm 6.6\%$ ) was found within the central regions of the infarct proper, an encouraging observation that suggests that the nascent myocardium may be well adapted for survival within the hostile environs of the scar. Although graft cells were generally separated from the host myocardium by scar tissue (Fig. 2c), most hearts showed occasional foci of close apposition of graft and host myocytes. These areas of host-graft contact showed shared adherens junctions at intercalated disk-like structures containing cadherin (Fig. 2f). (N-cadherin is the only cadherin known to be expressed in cardiomyocytes<sup>28</sup>, so this immunoreactivity most likely reflects N-cadherin content.) The human cardiomyocytes were smaller than the mature host cardiomyocytes and had immature but definite sarcomeric organization (Fig. 2g). The grafts also showed immunoreactivity for a variety of additional cardiac markers, including cardiac troponin I (Fig. 2g), the transcription factor Nkx2.5 (detected with a human-specific antibody in Fig. 2h), and myosin light chain 2V (Fig. 2i). Furthermore, the human cardiac grafts were uniformly negative for fast skeletal myosin heavy chain, a skeletal muscle marker (data not shown). Consistent with our earlier observations of hES cell-derived cardiomyocytes *in vitro*<sup>11</sup> or after transplantation in the uninjured heart<sup>13</sup>, the nascent myocardium that formed within the infarct zone was proliferating, as evidenced by the presence of occasional mitotic figures and by immunostaining for the thymidine analog 5-bromodeoxyuridine (BrdU), positive in  $1.4 \pm 0.2\%$  of the graft cardiomyocytes after a 1-h pulse (Supplementary Fig. 3 online). This proliferative index is slightly lower than that observed with implantation of embryoid body-derived cardiomyocytes in the uninjured heart model<sup>13</sup>, but it indicates that many of the hES cell-derived cardiomyocytes were still proliferating as long as 4 weeks after transplantation into the infarct.

Transplantation of undifferentiated murine ES cells into the heart results in cardiac teratomas rather than myocardial cells<sup>29,30</sup>. A careful search of all hearts in the current study revealed no teratomas or inappropriate tissue elements by routine morphology. Stains for ectoderm-derived neurons ( $\beta$ -III tubulin) and endoderm derivatives ( $\alpha$ -fetoprotein) were negative in every heart. We noted rare cytokeratin-positive epithelial cells in 4 of 15 hearts (accounting for  $0.5 \pm 0.3\%$  of the total human pan-centromeric-positive nuclei in hearts where present), but these did not form cysts, ducts or other recognizable tissues. In contrast to our previous experience with the implantation of less homogenous cardiac preparations into uninjured hearts (in which case the resultant grafts included a substantial quantity of human endothelial cells incorporated within chimeric capillaries<sup>13</sup>), grafts in the present study contained comparatively few human endothelial cells. Human endothelial cells, recognized with a human-specific CD31 antibody, were identified in 12 of 15 hearts and, where present, comprised a mean of only  $1.0 \pm 0.3\%$  of the total human nuclei. By contrast, the grafts had apparently induced a brisk, host-derived angiogenic response, as all of the cardiac implants contained numerous capillaries lined by rat endothelial cells (identified by the rat-specific endothelial marker RECA-1; see Supplementary Fig. 4 online).

None of the six hearts receiving the noncardiac hES cell-derived cells showed even a single human nucleus, as determined by staining with the human-specific pan-centromeric *in situ* probe. Similarly, immunostains for human cardiomyocytes (that is, human-specific Nkx2.5 antibody) and epithelial cells (the most common persistent noncardiac cell type in preceding studies<sup>13</sup>) were uniformly negative.

**Figure 2** Histological evaluation of human myocardial grafts at 4 weeks. Directly differentiated hES cell-derived cardiomyocytes were heat shocked and injected into 4 day-old infarcted rats, using the pro-survival cocktail to enhance survival. Panels a–c depict brightfield microscopic images from recipient hearts 4 weeks post-transplantation, whereas those in panels d–i were acquired with a three-laser confocal microscope. (a) Combined human pan-centromeric *in situ* hybridization and  $\beta$ -myosin heavy-chain immunostain. The implanted cells have formed a large graft of  $\beta$ -myosin-positive cardiomyocytes ( $\beta$ MHC, red stain) within the infarct scar tissue, and their human origin was confirmed by nuclear staining with the human-specific pan-centromeric *in situ* probe (huCent, brown chromagen). The left-ventricular cavity is at the upper right corner. Spared host subendocardial myocardium is present but is negative for  $\beta$ -myosin. Fast green counterstain. Scale bar, 100  $\mu$ m. (b) High magnification of boxed region in a. All of the  $\beta$ -myosin-positive cells (red stain) have nuclear staining with the pan-centromeric probe (huCent, brown-black stain), whereas rat nuclei in the surrounding scar or myocardial tissue are unstained. (c) Hematoxylin and eosin stain. A serial section to the boxed region in a is shown. The graft cells have a vacuolated appearance due to the presence of glycogen. Note the numerous nuclei in the rat scar tissue and spared myocardium, which were negative for the human pan-centromeric probe in the contiguous section presented in b. Scale bar, 50  $\mu$ m.

(d) Colocalization of human pan-centromeric *in situ* hybridization and  $\beta$ -myosin heavy chain. Co-localization of  $\beta$ -myosin heavy chain immunofluorescence (red signal) and the human-specific pan-centromeric probe (green) in the human cardiac grafts was confirmed by confocal microscopy. Note that the immediately adjacent rodent host myocardium shows minimal expression of  $\beta$ -myosin heavy chain. Scale bar, 100  $\mu$ m; inset shows the corresponding boxed area magnified twofold. (e) Graft and host myosin heavy chain expression pattern. This section was double-immunostained for sarcomeric myosin heavy chain (sMHC all striated muscle; red) and  $\beta$ -myosin heavy chain (human cardiac muscle; green). The human myocardial graft is clearly identified by the dual staining for sarcomeric and  $\beta$ -myosin, which appears yellow in this merged image. The surviving subendocardial rat myocardium is identified by the red staining for sarcomeric myosin. The surrounding infarct scar tissue is unstained. Scale bar, 100  $\mu$ m. (f) Host-graft contact. Infrequent but unequivocal sites of contact between host and graft myocardium were observed, as is illustrated by this section double-immunostained for  $\beta$ -myosin heavy chain (red) and cadherins (green). Points of close apposition between engrafted human myocardium (strongly immunoreactive for  $\beta$ -myosin heavy chain) and host muscle (minimally reactive) show shared adherens junctions, a component of intercalated disks, as indicated by cadherin staining (asterisks). Arrowheads indicate adherens junctions among the adjacent host cardiomyocytes. Scale bar, 10  $\mu$ m. (g) Cardiac troponin I expression and sarcomeric organization of graft cells. This section was double-immunostained for cardiac troponin I (green) and  $\beta$ -myosin heavy chain (red). Note that, in this merged image, the graft cells are positive for both markers and appear yellow, whereas the adjacent host cardiomyocytes only stain for cardiac troponin I (note green cells in lower right-hand corner). The graft muscle shows definite areas of sarcomeric organization (note boxed area, magnified twofold in inset). Scale bar, 20  $\mu$ m. (h) Combined Nkx2.5 and  $\beta$ -myosin heavy chain immunostain. This section was double-immunostained for  $\beta$ -myosin heavy chain (human cardiac muscle; green) and the cardiac-specific transcription factor Nkx2.5 (human-specific antibody; red nuclear signal). The human myocardial graft in the middle of the field is readily distinguishable by its strong positive reaction for both markers. Scale bar, 50  $\mu$ m. (i) Combined human pan-centromeric *in situ* hybridization and myosin light chain 2V immunostain. As demonstrated by this typical field, both host and graft (human-specific pan-centromeric positive, green nuclei) myocardium showed immunoreactivity for the ventricular-specific marker myosin light chain 2V (red). Scale bar, 20  $\mu$ m.



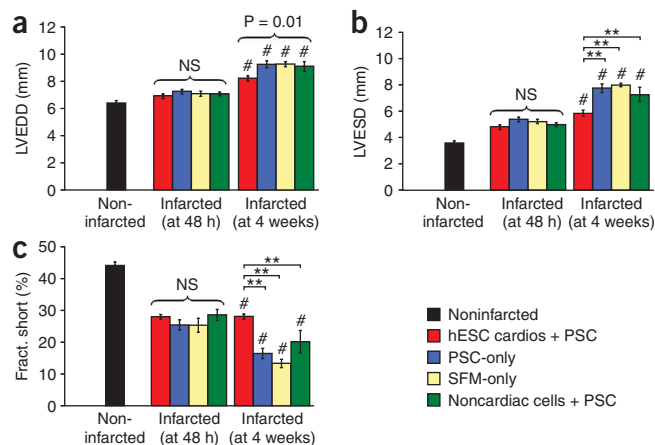
### Biodistribution of graft cells to distant organs

To investigate whether the transplanted hES cell derivatives migrated to and survived in organs other than the heart, we used quantitative PCR for human-specific ALU repetitive sequences to analyze brain, kidney, liver, lung and spleen tissues of rats receiving  $10 \times 10^6$  of these cells ( $n = 10$ ) or SFM ( $n = 3$ ). Standard curves demonstrated that this assay was capable of detecting a single human cell in a background of  $4 \times 10^5$  rodent cells. However, despite the sensitivity of this assay, the ALU qPCR analyses failed to detect any human genomes in all host tissues tested, indicating that there was little migration and survival of the ES cell derivatives in organs other than the heart.

### Graft effects on ventricular function

To determine the physiologic consequences of implanting direct-differentiated hES cell-derived cardiomyocytes in PSC into infarcted hearts, we compared the functional outcome with these cells to those observed with control hearts receiving either PSC only or SFM only. A third control of 'noncardiac' hES cell-derived cells was performed to specifically test the importance of using the highly cardiac-enriched preparation. To generate cells for this noncardiac control group, we subjected undifferentiated H7 hES cells to equivalent high-density monolayer culture conditions but omitted treatment with activin A and BMP4. These conditions

**Figure 3** Echocardiographic effects of hES cell-derived cardiomyocyte grafts on postinfarct ventricular function. Two days postinfarct, rats were studied by echocardiography to establish baseline structure and function and to ensure comparability among groups. Four days postinfarct, heat-shocked hES cell-derived cardiomyocytes were injected into the infarct, using the prosurvival cocktail (hES cell cardios+PSC, red bar) to enhance survival. Control rats received the prosurvival cocktail (PSC-only, blue bar), serum-free medium (SFM-only, yellow bar) in the absence of cells or noncardiac cells in PSC (green bar). Rats were then reevaluated by echocardiography at 4 weeks postinfarction. In addition, a separate cohort of uninjured rats was imaged to establish baseline values for the athymic rat (black bar). (a–c) Echocardiography results (for  $n = 11$  uninjured rats,  $n = 15$  infarcted rats receiving hES cell cardios+PSC,  $n = 16$  infarcted rats receiving PSC-only,  $n = 7$  infarcted rats receiving SFM-only and  $n = 6$  infarcted rats receiving noncardiac cells in PSC). (a) Left-ventricular end-diastolic dimension (LVEDD). All groups showed ventricular dilation at 48 h postinfarction, but there were no baseline differences among the groups (NS, no significant difference). Over the course of 4 weeks, each group dilated their LV end diastolic dimension compared with their paired, baseline value at 48 h (#,  $P < 0.05$ ). At 4 weeks, there was a trend toward reduced LVEDD in the hESC cardios + PSC group ( $P < 0.01$  by ANOVA), which did not reach significance by *post hoc* testing. (b) Left-ventricular end-systolic dimension (LVESD). All groups had comparably increased LVESD at 48 h postinfarction. Over the course of 4 weeks, each group dilated their LV end systolic dimension compared with their paired, baseline value at 48 h (#,  $P < 0.05$ ). At 4 weeks, hearts receiving hES cell-derived cardiomyocytes+PSC had significantly smaller LVESD compared with those receiving PSC-only, SFM-only, or noncardiac cells+PSC (\*\*,  $P < 0.01$  for all three comparisons). (c) Fractional shortening. All groups had comparable decreases in fractional shortening at 48 h postinfarction. Over the course of 4 weeks, each group except for the cardiac cell treated cohort exhibited a worsened fractional shortening compared with their paired, baseline value at 48 h (#,  $P < 0.05$ ). At 4 weeks, fractional shortening was significantly greater in the hearts receiving hES cell-derived cardiomyocytes compared with those receiving PSC-only, SFM-only or noncardiac cells+PSC (\*\*,  $P < 0.01$  for all three comparisons).



promoted differentiation but were poorly cardiogenic, and the resultant cells contained only a mean of 0.8% cardiomyocytes. Recipients of these 'noncardiac' cells were otherwise equivalently treated, that is, receiving  $10 \times 10^6$  of the heat-shocked noncardiac

hES cell derivatives in the presence of PSC 4 d postinfarction. All physiological studies were conducted and interpreted by investigators who were blinded to the animal's treatment (**Supplementary Table 1** online).

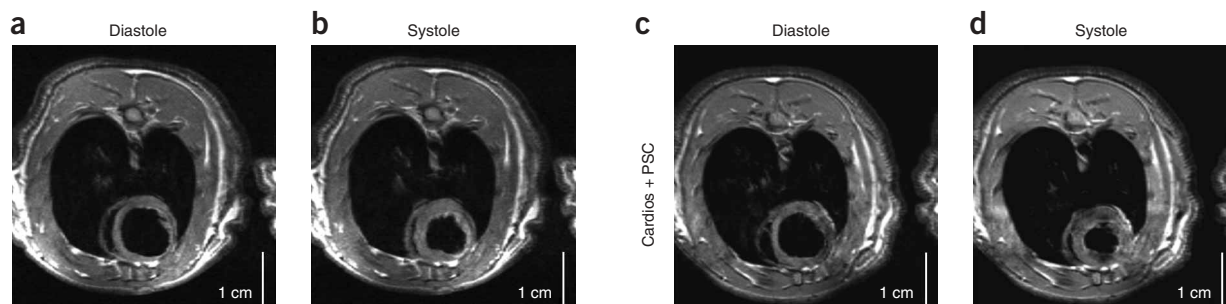
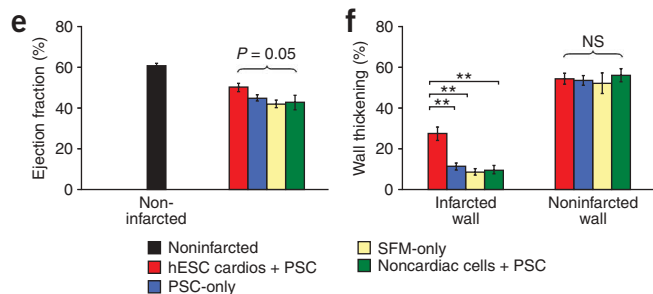


**Figure 4** Evaluation of the effects of hES cell-derived cardiomyocyte grafts on postinfarct ventricular function by magnetic resonance imaging (MRI). (a–d) Representative short-axis  $^1\text{H}$  MR images show hearts receiving hES cell-derived cardiomyocytes in presence of the prosurvival cocktail (hES cell+PSC, c,d) or the cocktail alone (PSC-only, a,b). Hearts are shown at end-diastole (a,c) and end-systole (b,d). Note the reduced ventricular dilation as well as greater systolic thickening of the anterior wall in the heart treated with hES cell+PSC compared to PSC-only. Scale bar, 1 cm. The orientation is dorsal-up, ventral-down. (e,f) Quantitative MRI assessments of left-ventricular ejection fraction and wall thickening for noninfarcted rats ( $n = 9$ , black bars), as well as for the infarcted rats receiving hES cell cardios + PSC ( $n = 15$ , red bars), PSC-only ( $n = 10$ , blue bars), SFM only (SFM-only,  $n = 5$ , yellow bars) and noncardiac cells+PSC ( $n = 6$ , green bars). (e) Left-ventricular ejection fraction (LVEF). Transplantation of hES cell-derived cardiomyocytes was associated with a higher ejection fraction, though at a borderline statistical significance ( $P = 0.05$ ). *Post hoc* analysis demonstrates cardio-treated cohort to have better LVEF versus PSC-only ( $*P < 0.05$ ) or SFM-only ( $**P < 0.01$ ) treated animals. (f) Regional wall thickening. Wall thickening was determined by MRI in the thinnest region of the infarct in the four apical-most slices, as well as in the noninfarcted interventricular septum. Transplantation of hES cell-derived cardiomyocytes caused an ~2.5-fold increase in systolic wall thickening in the infarcted zone relative to PSC-only, SFM-only and noncardiac cell+PSC (\*\*,  $P < 0.01$  for all) controls, indicating greater contractile activity resulted from cardiac cell transplantation. By contrast, wall thickening in the noninfarcted segment did not differ among groups.



Echocardiography (Fig. 3a–c) demonstrated that lightly anesthetized, noninfarcted athymic rats had left-ventricular end diastolic dimensions (LVEDD) of  $6.4 \pm 0.1$  mm, left-ventricular end systolic dimensions (LVESD) of  $3.6 \pm 0.1$  mm and fractional shortening (FS) of  $44 \pm 1\%$ . Two days after infarction (but 2 d before cell transplantation), all groups showed ventricular dilation and reduced fractional shortening, but there were no differences among groups. Overall, at 2 d postinfarction LVEDD increased by  $\sim 10\%$ , LVESD increased by  $\sim 42\%$  and fractional shortening decreased by  $\sim 40\%$ .

By 28 d after hES cell-derived cardiomyocyte or vehicle injection, all groups showed progressive ventricular dilation relative to their baseline studies 2 d after infarction (Supplementary Fig. 5 online). There was a trend toward an attenuation of the increase in LVEDD in hearts receiving hES cell-derived cardiomyocytes versus controls (Fig. 3a), but this effect did not reach statistical significance. (ANOVA indicated that LVEDD differed among the four cohorts ( $P = 0.01$ ), but no significant difference was found by *post hoc* testing.) All four groups showed increased LVESD over 28 d, but this increase was markedly attenuated in hearts receiving hES cell-derived cardiomyocytes (Fig. 3b). LVESD in cardiomyocyte-engrafted hearts was  $5.8 \pm 0.2$  mm versus  $7.7 \pm 0.3$  mm in PSC only,  $8.0 \pm 0.1$  mm in SFM-only and  $7.3 \pm 0.5$  mm in noncardiac cell receiving rats ( $P < 0.01$  for all control groups versus cardiac cell-treated cohort). There was no difference in LVESD among PSC, SFM or noncardiac cell control groups at 4 weeks.

Left-ventricular systolic function, measured by fractional shortening, declined significantly in control hearts over the 4-week test period, decreasing to  $16.5 \pm 1.7\%$  in PSC-only hearts,  $13.4 \pm 1.3\%$  in hearts receiving SFM, and  $20.3 \pm 3.5\%$  in the noncardiac cell-treated group. ( $P < 0.05$  for pair-wise comparison of each group at  $-2$  d versus 28 d). There was no difference in fractional shortening among the three control cohorts at 28 d. In contrast, transplantation of hES cell-derived cardiomyocytes completely prevented the decline in fractional shortening (Fig. 3c). In the cardiac cell-treated hearts, fractional shortening at day  $-2$  was  $28.2 \pm 0.7\%$  versus  $28.4 \pm 1.5\%$  at day 28 ( $P = 0.98$  for  $-2$  d versus 28 d). At 28 d after engraftment, the cohort treated with hES cell-derived cardiomyocytes had significantly greater fractional shortening compared with noncardiac cells, PSC-only and SFM-only controls ( $P < 0.01$  for all control cohorts versus cardiac cell-treated group).

Assessment of the rat heart function by MRI confirmed the expected changes in heart function and geometry by 4 weeks after infarction: left-ventricle chamber dimensions were significantly increased, and ejection fraction was reduced in all hearts as compared with control noninfarcted animals ( $P < 0.01$ , Supplementary Table 1). However, transplantation of hES cell-derived cardiomyocytes into infarcted recipients significantly attenuated the changes in left-ventricle geometry and improved cardiac function. In particular, left-ventricle chamber volumes at end-systole (LVESV) and end-diastole (LVEDV) were decreased in the cardiac cell-treated group compared with the SFM-only group ( $*P < 0.05$ , Supplementary Table 1), and there was a similar positive trend relative to other controls (Fig. 4a–d). ANOVA demonstrated a statistically borderline effect ( $P = 0.05$ ) of cardiomyocyte transplantation on ejection fraction when all four groups were compared (Fig. 4e). Ejection fraction was  $50.3 \pm 2\%$  in hearts receiving cardiomyocytes plus PSC versus  $45 \pm 1.6\%$  in those receiving PSC only,  $42 \pm 1.9\%$  in SFM only and  $43 \pm 4\%$  with noncardiac cells. *Post hoc* comparison of the groups revealed significant differences between cardiomyocytes plus PSC versus PSC only or SFM only.

The effects of human cardiomyocyte transplantation were most apparent after analysis of the regional contractile function. In the infarct region of cardiomyocyte-engrafted hearts, left-ventricle wall thickening averaged  $27.5 \pm 3.3\%$ , compared with  $11.5 \pm 1.9\%$  in the PSC-only group,  $8.8 \pm 1.7\%$  in the SFM-only group or  $9.8 \pm 2.0\%$  in the group receiving noncardiac cells ( $**P < 0.01$  for each control versus cardiac cell-treated cohort). Wall thickening in the noninfarcted region was comparable among all four groups (Fig. 4f). Taken together, these data indicate that formation of human myocardium in the infarcted rat heart significantly attenuates the progression of heart failure, manifested by reduced ventricular dilation (LVESD, LVEDD), improved global function (fractional shortening and ejection fraction) and increased regional wall motion compared with controls receiving noncardiac cells or vehicle.

## DISCUSSION

This study demonstrates that transplanted hES cell-derived cardiomyocytes can positively influence cardiac structure and contractile function after myocardial infarction. Previous studies have demonstrated that hES cell-derived cardiomyocytes can form human myocardium after transplantation into the noninfarcted hearts of athymic rats<sup>13</sup> or immunosuppressed pigs<sup>14</sup>. When hES cell-derived cardiomyocytes are implanted in slow heart-rate species, such as pigs or guinea pigs, they can form pacemakers when the native one is dysfunctional<sup>14,15</sup>, implying electrical integration with surrounding myocytes.

In our study, most of the hES cell-derived cardiomyocytes initially died after transplantation into the infarcted heart. This problem is not unique to our system. Death of transplanted cells is slowing research progress in cell therapy for diabetes<sup>31,32</sup>, Parkinson's disease<sup>33,34</sup> and muscular dystrophy<sup>35,36</sup>, among other diseases. We found that cardiomyocyte death was multifactorial in origin. Single interventions had little impact on engraftment and no impact on cardiac function, but the combinatorial intervention resulted in reliable formation of substantial myocardial grafts. Matrigel was shown to make an independent contribution, suggesting anoikis is a significant initiator of cell death. We suspect there are additional stimuli for death not targeted by our PSC. Current studies are focused on identifying additional death pathways and sorting out the relative importance of each of the components in the cocktail, but the PSC described here is currently our best formulation. To the extent that cell death after transplantation has common mechanisms, the PSC formulation (or similar variations) might prove broadly applicable to other candidate cell preparations for regenerative medicine.

Virtually all of the noncardiac hES cell-derived cells died by the 4-week time point despite delivery in PSC. Although the mechanisms underlying this difference from the cardiomyocyte grafts (in which case all hearts receiving myocytes showed surviving cells) are unclear, there is some precedence for this finding. In earlier work involving the transplantation of preparations of lower cardiac purity into uninjured hearts, we found that the contaminating noncardiac cells were efficiently cleared from the recipient heart, suggesting that some cell-intrinsic or environmental factor(s) favored cardiomyocyte survival. Although clearance of nonmyocytes was less reliable in infarcted hearts (Supplementary Fig. 1), it is clear that not every hES cell derivative will persist after cardiac transplantation.

The most important observation in the present study is that engraftment of hES cell-derived cardiomyocytes improved cardiac function. This raises questions about the mechanisms underlying this effect. The most straightforward explanation is that the implanted human cardiomyocytes beat synchronously with the host myocardium and thereby directly contribute systolic force. In support of this,

the infarcted walls of hearts receiving the highly enriched hES cell-derived cardiomyocytes showed 2.5-fold greater thickening during systole as compared to controls (Fig. 4f). Greater wall thickening implies more local force-generating units across the infarct wall, which could arise directly from the human cardiomyocytes. Alternatively, the force could have been generated by host cells indirectly influenced by the transplanted human cells. There is evidence that transplanted cells produce paracrine factors that enhance survival of host cardiomyocytes postinfarction<sup>37–39</sup>. Paracrine factors may also enhance angiogenesis, improve the extracellular matrix or modulate the immune/inflammatory response<sup>40,41</sup>. Notably, all groups had comparable infarct sizes, which rules out an effect on infarct healing and scar shrinkage. Our data suggest that, if paracrine mechanisms play a role, they may be specific to cardiomyocytes, as nonmyocytes did not increase systolic function and showed only modest trends toward reducing ventricular dilation. Tethering of engrafted cardiomyocytes to host myocardium through the extracellular matrix or intercellular junctions makes it difficult to assess the grafts' direct mechanical effects, even using high-resolution MRI. It will be important to directly determine whether the grafts are electromechanically active *in vivo*, for example, through intravital calcium imaging<sup>42,43</sup>. If the grafts are not beating synchronously, this would imply that a paracrine mechanism is responsible. It would also imply that an additional increment of improvement is possible when hES cell-derived cardiomyocytes are delivered to hearts of larger species with slower heart rates, including humans.

The directed differentiation system employed here involving serial application of activin A and BMP4 was developed in response to the need for a clinically scalable system for human cardiomyocyte growth. The selection of these particular factors and the timing of their application were based on previous work in model systems. Activin was originally shown to be an effective inducer of mesoderm and endoderm in *Xenopus* embryonic explants<sup>44</sup>, and analysis of factors secreted by the chick hypoblast and anterior endoderm indicated that the transforming growth factor (TGF) $\beta$  family of secreted factors are expressed at the appropriate stages of development (activin A and TGF $\beta$  in the hypoblast; BMPs in the anterior endoderm) to play a role in cardiac induction<sup>45–49</sup>. We therefore hypothesized that exposure of undifferentiated hES cells to activin would induce generic mesoderm and that subsequent BMP4 would further specify the cardiac fate. Indeed, this activin/BMP4-directed differentiation system proved robustly cardiogenic, was at least 50-fold more efficient than the use of embryoid bodies with serum induction<sup>50</sup> and gave more consistent yields and purities. Nonetheless, human hearts will clearly need proportionately larger cell preparations. Current work indicates that the activin/BMP system scales to larger formats with only minor modifications (J.G. and Y. Li, unpublished observations). This makes large-animal studies realistic and suggests scalability to humans should be possible. Of course, success in the scaled production of these cells will require an improved understanding of the molecular events in hES cell self-renewal and early cardiac differentiation<sup>51–53</sup>, as well as the identification of novel approaches to optimize the maintenance<sup>54</sup>, enrichment<sup>55–57</sup>, proliferation<sup>11</sup> and maturation of hES cell-derived cardiomyocytes *in vitro*.

Testing hES cell-derived cardiomyocytes in a rat xenotransplant model has several limitations. Many issues related to immunogenicity would be expected to differ compared with human allogeneic transplantation. Also, the rat's high heart rate could mask arrhythmias generated by pacemaker activity or re-entrant circuits that would occur in slower heart rate species. We observed no increased mortality in rats receiving human cardiomyocytes compared to controls, but

studies in species with slower heart rates will be required to test for arrhythmias. Finally, the effectiveness of human cardiomyocytes might be underestimated in the rat if they cannot keep pace with the rat myocytes but could in larger species.

The ability of human cardiomyocytes to improve structure and function in the infarcted rat heart provides important proof of concept for this cell type. Future studies are required to better understand the mechanisms responsible and to test the ability of these cells to repair hearts under conditions that closely match human disease.

## METHODS

**Preparation of hES cell-derived cardiomyocytes.** All studies used cells derived from the female H7 human ES cell line<sup>58</sup>, which was maintained in the undifferentiated state at Geron Corporation using mouse embryonic fibroblast conditioned medium (MEF-CM), as previously described<sup>59</sup>. For most described experiments, hES cell-derived cardiomyocytes were generated using our recently reported protocol for efficient cardiogenesis<sup>57</sup>. In brief, undifferentiated hES cells were detached by a 10-min incubation with 0.5 mM EDTA or 200 U/ml collagenase IV (Worthington Biochemical) and seeded onto Matrigel-coated plates (Growth Factor Reduced Matrigel, BD Biosciences) at a density of 100,000 cells/cm<sup>2</sup>. Cells were refed daily with MEF-CM plus 8 ng/ml basic fibroblast growth factor (bFGF) for 6 d. To induce cardiac differentiation, we replaced MEF-CM with RPMI-B27 medium (Invitrogen) supplemented with the following cytokines: 100 ng/ml human recombinant activin A (R&D Systems) for 24 h, followed by 10 ng/ml human recombinant BMP4 (R&D Systems) for 4 d. The medium was then exchanged for RPMI-B27 without supplementary cytokines; cultures were refed every 2–3 d for 2–3 additional weeks. Widespread spontaneous beating activity was typically observed by day 12 after addition of activin A. For control experiments involving 'noncardiac' preparations, hES cells were differentiated under otherwise identical culture conditions, but activin A and BMP4 were omitted. Some of the early experiments to validate the PSC were performed before the development of the directed cardiac differentiation protocol. Thus, for the experiments depicted in Figure 1 (that is, experiments with 1-week histological endpoints only), hES cell-derived cardiomyocytes were generated using the far less cardiogenic, 'standard' embryoid body culture protocol, using techniques that we have previously reported<sup>8,13</sup>.

After either 2 weeks (directed differentiation protocol) or 3 weeks (embryoid body protocol) of *in vitro* differentiation, cultures were shipped overnight to the University of Washington for implantation studies. After receipt and 3–4 d of recovery in their usual medium, cultures were subjected to transient heat-shock (with a 30-min exposure to 43 °C medium), followed by a return to either control medium or, for PSC-treated cells, medium supplemented with IGF-1 (100 ng/ml) and cyclosporine A (0.2  $\mu$ M). Twenty-four hours later, cells were enzymatically dispersed for implantation using Blendzyme IV (Roche, prepared at 0.56 U/ml in PBS) and DNase (Invitrogen, 60 U/ml) for 30 min at 37 °C and enriched for cardiomyocytes by separation over a discontinuous Percoll gradient, using previously detailed methods<sup>8,11,13</sup>. The resultant cardiomyocyte-enriched fractions (that is, the denser fractions III and IV) were used for transplantation studies. Note that noncardiac control cells were not Percoll enriched, but they were otherwise equivalently processed (including preceding heat shock, IGF-1 and cyclosporine treatment.) Cell preparations to be transplanted were enzymatically dispersed to small clusters of less than ten cells, which were suspended in a 70- $\mu$ l volume per rat of either serum-free medium (SFM group, using RPMI medium (Invitrogen) without B27), Matrigel (Matrigel-only group, using 50% (vol/vol) Matrigel/cells+RPMI medium) or the full PSC, including Matrigel. The full PSC cocktail consisted of 50% (vol/vol) growth factor-reduced Matrigel, supplemented with ZVAD (100  $\mu$ M, benzyloxycarbonyl-Val-Ala-Asp(O-methyl)-fluoromethyl ketone, Calbiochem)<sup>60,61</sup>, Bcl-X<sub>L</sub> BH4 (cell-permeant TAT peptide, 50 nM, Calbiochem)<sup>60–62</sup>, cyclosporine A (200 nM, Wako Pure Chemicals)<sup>22,63,64</sup>, IGF-1 (100 ng/ml, Peptotech)<sup>65,66</sup> and pinacidil (50  $\mu$ M, Sigma)<sup>67–69</sup>.

To ensure comparable cardiac purity among preparations, we routinely plated-out (50,000 cells/cm<sup>2</sup>) a small subset of the cells to be implanted on

gelatin-coated substrates and cultured them for 48 h before fixation and immunostaining for  $\beta$ -myosin heavy chain. This analysis, which may underestimate the cardiac purity of the input population (e.g., due to fibroblast overgrowth) revealed the Percoll-enriched cells to be  $82.6 \pm 6.6\%$  cardiomyocytes (range 71–95%). Equivalently prepared cells have been examined for the presence of skeletal muscle cells many times and have been found uniformly negative (data not shown). Cell preparations resulting from Percoll-enriched embryoid body cultures consistently contained  $\sim 15\%$  cardiomyocytes. Control 'noncardiac' preparations (that is, made by subjecting hES cells to the aforementioned direct differentiation procedure but omitting activin A, BMP4 and Percoll enrichment) contained a mean of only 0.8% cardiomyocytes.

**Myocardial infarction and cell implantation.** All studies were approved by the University of Washington Animal Care and Use Committee and were conducted in accordance with federal guidelines. The protocol for cell implantation has been detailed in multiple previous reports by our group<sup>13,70,71</sup>. We chose the athymic nude rat as a host because of its well-established history in xenotransplantation and the comparative ease and reliability of physiologic studies in the rat. In brief, athymic male Sprague Dawley rats (rh rnu-rnu, 240–300g, Harlan) were anesthetized with an intraperitoneal injection of 70–100 mg/kg ketamine (Phoenix Pharmaceuticals) and 7–10 mg/kg xylazine (Phoenix Pharmaceuticals), intubated and mechanically ventilated with room air supplemented with oxygen. The heart was exposed by an open thoracotomy and subjected to 60 min of ischemia-reperfusion injury by temporary ligation of the left anterior descending artery by 7-0 Prolene suture. Two days after recovery from this procedure, animals underwent echocardiographic evaluation as detailed below.

Animals meeting the echocardiographic inclusion criterion (fractional shortening  $< 40\%$ ) were stratified to one of four groups: those receiving intracardiac injections of hES cell-derived cardiomyocytes suspended in PSC, the noncardiac cells suspended in PSC, PSC-only or SFM only. These implantations were performed 4 d after the initial ischemia-reperfusion infarct (2 d after echocardiography). On the day of engraftment, the rats were again anesthetized with ketamine/xylazine, mechanically ventilated and subjected to a second thoracotomy followed by direct injection of 70  $\mu$ l of agent (hES cell-derived cardiomyocytes in PSC versus noncardiac cells in PSC versus PSC-only versus SFM-only) using a Hamilton syringe (Hamilton Company) and a 30-gauge needle. To better ensure exposure of implanted cells to therapeutic levels of cyclosporine A throughout the period in which graft cell death would be expected to be maximal, all cell-treated and PSC-only control rats received daily subcutaneous injections of cyclosporine A (0.75 mg/day, Wako Pure Chemicals), starting 1 d before engraftment and continuing for 7 d after engraftment.

Four weeks after implantation, the surviving rats were analyzed by repeat echocardiography and MRI (described below) and then were killed with Beuthanasia (1.5–2 ml intraperitoneal injection, Schering-Plough). One hour before, rats received an intraperitoneal pulse of 5-bromodeoxyuridine (BrdU, 1.0 ml of a 10 mg/ml solution, prepared in PBS) to mark cells synthesizing DNA. The heart and various organs were harvested, immersion-fixed in methyl Carnoy's solution and processed for histological analysis.

**Echocardiography.** Two days after the ischemia-reperfusion infarction and 2 d before engraftment, the animals were lightly anesthetized with inhaled isoflurane (Novaplus) and scanned by transthoracic echocardiography (GE Vivid 7) with a 10S (10 MHz) pediatric probe to record physiological data and to stratify the rats by left-ventricular systolic function. Specifically, the left-ventricular end diastolic dimension (LVEDD), the left-ventricular end systolic dimension (LVESD) and heart rate were measured and recorded. Fractional shortening, an index of LV systolic function, was calculated by this equation:  $FS = 100 \times (LVEDD - LVESD) / LVEDD$ . Rats with fractional shortening  $> 40\%$  were excluded from the study. LVEDD and LVESD are expressed in mm. Heart rate is expressed in beats per minute. As noted above, repeat echocardiographic analyses were performed 4 weeks after implantation. All investigators performing echocardiographic acquisition or analysis were blinded to treatment group.

**Magnetic resonance imaging (MRI).** Four weeks after implantation, the cardiac function of rats was also evaluated by high-resolution MRI using a 4.7T Varian scanner. Rats were anesthetized with 1.5% isoflurane in oxygen (1 l/min) delivered through a nose cone, and placed in a custom-constructed

<sup>1</sup>H transmit-receive volume coil on a flat Plexiglas platform. Needle electrodes were attached to the animal's extremities for ECG monitoring and to trigger the MRI acquisitions using commercially available software (Small Animal Monitoring and Gating System, SA Instrument). High-resolution spin-echo transverse <sup>1</sup>H MR images were obtained to quantify left-ventricular function (field of view: 50 mm<sup>2</sup>; 2D matrix: 256  $\times$  128; TR: 400 ms; TE: 13 ms; flip angle: 90°, two signal averages). A set of multislice short-axis images (slice thickness 1.5 mm without gap between slices) for end-systole and another for end-diastole were acquired.

Epicardial and endocardial borders were manually traced for calculation of left-ventricle volumes at end-systole and end-diastole (LVESV, LVEDV) and left-ventricular mass (LVmass) using the software package NIH ImageJ version 1.34s. Total LV volumes were calculated as the sum of all slice volumes. The left-ventricular ejection fraction (LVEF) was calculated by the equation  $(LVEDV - LVESV) / LVEDV \times 100\%$ . Left-ventricle wall thickening was measured in the central infarcted region and in the noninfarcted mid-septal wall, using averages obtained from the four apical-most slices for each heart. Wall thickening was then calculated as the relative difference in LV wall thickness in end-systole and end-diastole and expressed as a percentage of end-diastolic thickness. Investigators performing MRI acquisition and analysis were blinded to treatment group assignment.

**Histology, immunocytochemistry and *in situ* hybridization.** To ensure that we achieved equivalent sampling, all hearts were fixed and vibratome-sectioned to 1-mm thickness, and the resultant uniform transverse sections were routinely processed and paraffin-embedded for histology. Five-micrometer sections were then stained with hematoxylin-eosin and picosirius red/fast-green (to determine infarct area), as well as subjected to *in situ* hybridization and immunohistochemistry using previously detailed methods<sup>13,72</sup>. Immunostaining was performed with antibodies directed against the muscle antigens sarcomeric myosin heavy chain (clone MF-20, Developmental Studies Hybridoma Bank), the  $\beta$ -myosin heavy chain isoform (clone A4.951, American Type Culture Collection), pan-cadherins (rabbit polyclonal, Sigma), cardiac troponin I (clone 19C7, Abcam), human Nkx2.5 (goat polyclonal, R&D) and myosin light chain 2V (rabbit polyclonal). To evaluate for the presence of noncardiac graft elements, we also immunostained with antibodies against the following cell types: neurons ( $\beta$ III-tubulin), endoderm ( $\alpha$ -fetoprotein, Dako), epithelium (pan-cytokeratin cocktail (AE1/AE3, Dako)), endothelium (human-specific CD31/PECAM, Dako; *Ulex europaeus*, Vector) and skeletal muscle (fast skeletal myosin heavy chain, MY32 clone, Sigma). Host-derived endothelium was identified with a rat-specific anti-endothelial antibody (rat endothelial cell antigen-1, Abcam). Proliferation was assessed by immunostaining for incorporated BrdU (peroxidase-conjugated mouse anti-BrdU monoclonal antibody, Roche).

The engrafted human cells were identified using *in situ* hybridization with a human-specific pan-centromeric genomic probe<sup>13,18</sup>. All evaluated sections were either double-labeled with this human-specific marker or an immediately contiguous section was so-labeled. The human-specific pan-centromeric probe is generated by modification of a protocol previously reported<sup>18</sup> that involves degenerate PCR with primers against human centromeric sequences. We then labeled the PCR product with digoxigenin (Dig Hi-Prime labeling kit, Roche), which was subsequently detected after *in situ* hybridization using a peroxidase-conjugated anti-digoxigenin antibody (Roche). For brightfield studies involving *in situ* hybridization with the pan-centromeric probe, chromagenic detection of the *in situ* probe was performed with diaminobenzidine (Sigma) and any preceding immunohistochemistry used Vector Red (Vector Labs) for detection. For studies requiring confocal microscopy, the *in situ* probe was detected by Alexa Fluor 488 tyramide (Molecular Probes), again with preceding immunohistochemistry detected by the intrinsic red fluorescence of the Vector Red deposit.

Note that, when performed on tissue fixed with methyl Carnoy's, the *in situ* hybridization procedure unfortunately precludes subsequent staining with all available nuclear counterstains. For this reason, we used fast green (cytoplasmic) counterstaining in all brightfield *in situ* studies and no counterstain in fluorescent *in situ* studies. In studies not involving *in situ* hybridization, nuclear counterstaining was done using either routine hematoxylin (brightfield) or Hoechst 33342 (fluorescence) dyes. It also is worth noting that, in studies

employing the human-specific *in situ* probe in combination with a second cardiac marker (usually  $\beta$ -myosin heavy chain), fine structural details, such as sarcomeric organization, can become difficult to appreciate. First, the relatively rough treatments to the tissue (that is, acid and proteinase treatment, high temperatures to denature target DNA sequences) necessary for *in situ* hybridization subtly distort the tissue architecture. Second, we have found the only preceding reporter that reliably survives the *in situ* hybridization procedure is the chromagen Vector Red, and so, when we have used a second marker, it has been detected with this stain. Vector Red is an enzymatic substrate and so generally does not have the crisp staining pattern possible with a directly conjugated secondary antibody. For these reasons, when doing studies to specifically evaluate the sarcomeric organization of the grafts, we have performed immunofluorescence only, relying on *in situ* hybridization for the human marker on an adjacent section as well as  $\beta$ -myosin heavy chain or human-specific Nkx2.5 immunostaining in the same section (Fig. 2g).

Whereas all grafts were confirmed by the human-specific *in situ* probe, the human ES cell-derived cardiac implants were also quite distinct morphologically and also could be readily distinguished from the host on the basis of their exclusive immunoreactivity for  $\beta$ -myosin heavy chain, as opposed to the rodent host ventricular myocardium, which expressed  $\alpha$ -myosin heavy chain. We found all strongly  $\beta$ -myosin heavy chain positive cells to be positive for the human-specific *in situ* probe. We further confirmed this expected pattern of myosin heavy chain expression on a subset of cell-engrafted hearts using immunofluorescent colocalization by confocal microscopy. For this, sections were double-immunostained using antibodies recognizing  $\beta$ -myosin heavy chain (A4.951 monoclonal primary, followed by tyramide amplification with a sheep anti-mouse IgG HRP-conjugated secondary antibody (Amersham) and Alexa Fluor 488 tyramide (Molecular Probes)) and sarcomeric (that is,  $\alpha$ - and  $\beta$ -) myosin heavy chains (MF-20 monoclonal primary, followed by a biotinylated goat anti-mouse (Vector) and streptavidin-conjugated Alexa 555 (Molecular Probes)). Sections showing close apposition of graft and host muscle were similarly analyzed by confocal microscopy for the presence of shared intercalated disc structures, using dual immunofluorescent labeling for  $\beta$ -myosin heavy chain and cadherins. Similar dual immunofluorescent labeling studies were performed combining  $\beta$ -myosin heavy chain with cardiac troponin I and Nkx2.5. In all cases, slides were then counterstained with Hoechst nuclear dye, mounted with Vectashield (Vector), and visualized on Zeiss LSM510 META confocal microscope using a 10 $\times$ , 40 $\times$  and 63 $\times$  objectives.

All quantitative histologic studies were performed in a blinded fashion using brightfield microscopy. Cell nuclei counts were obtained using an Olympus BX41 microscope with a 40 $\times$  objective. Morphometric analyses were performed by acquiring digital photomicrographs of all vibratomed profiles with the stain of interest (with an Olympus SZ-PT dissecting microscope equipped with a Nikon Coolpix 995 digital camera) and then measuring areas using Adobe Photoshop. Morphometric determinations of infarct size were expressed as the percentage of total left-ventricular cross-sectional area occupied by picosirius red-positive infarct zone. Graft size was expressed as the percentage of picosirius red-positive infarct area occupied by human  $\beta$ -myosin heavy chain positive graft.

**Biodistribution analysis: quantitative real time PCR (qPCR) for human ALU sequences.** To investigate whether derivatives of the transplanted cells migrated to and survived in other organs, we analyzed brain, kidney, liver, lung and spleen tissue of rats transplanted with hES cell-derived cardiomyocytes ( $n = 10$ ) and SFM ( $n = 3$ ) at the 4-week time point. The human ALU PCR primer were as follows (5'  $\rightarrow$  3'): GTCAGGAGATCGAGACCATCCC (forward) and TCCTGCCTCAGCCTCCCAAG (reverse)<sup>73</sup>. Samples were run on Applied Biosystems (AB) 7900HT Fast Real Time PCR System using AB PowerSybr-Green 2 $\times$  mastermix. Assuming a value of 5 pg DNA per cell<sup>74</sup>, standard curves demonstrated that the assay detected a single human cell (5 pg DNA) in samples containing a constant background of  $4 \times 10^5$  rodent cells ( $= 200$  ng DNA). We tested 1  $\mu$ g of the various organ-specific genomic DNA for each animal and samples were run in triplicates.

**Statistics.** For analysis involving three or more groups, we used ANOVA followed by Student-Newman-Keuls *post hoc* testing (Sigma Stat, 2006) with

$\alpha = 0.05$  for significance. For analysis of time course changes in LV size, LV function and HR, a paired *t*-test analysis of means was used. All data were analyzed in a blinded manner, with the breaking of the identifier code only after the data were acquired. Values are expressed as means  $\pm$  s.e.m., unless otherwise stated.

*Note: Supplementary information is available on the Nature Biotechnology website.*

#### ACKNOWLEDGMENTS

The authors thank Lil Pabon for helpful scientific discussions and Vasily Yarnykh and Eric Shankland for support of our magnetic resonance imaging studies. We are indebted to Kellie Schurb for assistance with animal surgery, to Mark Saiget for assistance with ALU qPCR and to Ron Hanson for managerial support of the project. We thank Jane Lebkowski for her ongoing support of this research collaboration. We thank K. Chien for myosin light chain 2V, rabbit polyclonal. This study was supported in part by a grant from Geron and in part by National Institutes of Health grants P01 HL03174, R01 HL061553, R01 HL084642, P20 GM069983 (to C.E.M.), R24 HL064387 (to C.E.M. and M.A.L.), T32 HL07828 (to M.A.L. and K.Y.C.), K08 HL080431 (to M.A.L.) and T32 EB001650 (to A.V.N.).

#### AUTHOR CONTRIBUTIONS

M.A.L. and K.Y.C. were the principal experimentalists and contributed to the writing of the manuscript. A.V.N. performed the MRI scans and contributed to the writing. V.M. performed most of the histology and microscopy. J.A.F. cultured hES-derived cardiomyocytes and prepared cells for transplant. S.K.D. performed surgeries and *in situ* hybridization. H.R. performed the biodistribution studies. C.X., M.H., S.P., C.O., L.C. and J.G. generated hES-derived cardiomyocytes and prepared cells for transplant. Y.C. performed surgeries. E.M., E.A.G. and S.U. performed the echocardiography. J.G. designed experiments and contributed to the writing of the manuscript. C.Y. coordinated the MRI studies. C.E.M. designed experiments, coordinated the project and contributed to the writing of the manuscript.

#### COMPETING INTERESTS STATEMENT

The authors declare competing financial interests: details accompany the full-text HTML version of the paper at <http://www.nature.com/naturebiotechnology/>.

Published online at <http://www.nature.com/naturebiotechnology/>

Reprints and permissions information is available online at <http://npg.nature.com/reprintsandpermissions>

- Mallory, G.K., White, P.D. & Salcedo-Salgar, J. The speed of healing of myocardial infarcts: a study of the pathologic anatomy in seventy-two cases. *Am. Heart J.* **18**, 647–671 (1939).
- Rumiantsev, P. *Growth and Hyperplasia of Cardiac Muscle Cells* (Harwood, London/New York, 1991).
- Pasumathi, K.B. & Field, L.J. Cardiomyocyte cell cycle regulation. *Circ. Res.* **90**, 1044–1054 (2002).
- Rubart, M. & Field, L.J. Cardiac regeneration: repopulating the heart. *Annu. Rev. Physiol.* **68**, 29–49 (2006).
- Laflamme, M.A. & Murry, C.E. Regenerating the heart. *Nat. Biotechnol.* **23**, 845–856 (2005).
- Dimmeler, S., Zeiher, A.M. & Schneider, M.D. Unchain my heart: the scientific foundations of cardiac repair. *J. Clin. Invest.* **115**, 572–583 (2005).
- Murry, C.E., Field, L.J. & Menasche, P. Cell-based cardiac repair: reflections at the 10-year point. *Circulation* **112**, 3174–3183 (2005).
- Xu, C., Police, S., Rao, N. & Carpenter, M.K. Characterization and enrichment of cardiomyocytes derived from human embryonic stem cells. *Circ. Res.* **91**, 501–508 (2002).
- Mummery, C. *et al.* Differentiation of human embryonic stem cells to cardiomyocytes: role of coculture with visceral endoderm-like cells. *Circulation* **107**, 2733–2740 (2003).
- Kehat, I. *et al.* Human embryonic stem cells can differentiate into myocytes with structural and functional properties of cardiomyocytes. *J. Clin. Invest.* **108**, 407–414 (2001).
- McDevitt, T.C., Laflamme, M.A. & Murry, C.E. Proliferation of cardiomyocytes derived from human embryonic stem cells is mediated via the IGF/PI 3-kinase/Akt signaling pathway. *J. Mol. Cell. Cardiol.* **39**, 865–873 (2005).
- Snir, M. *et al.* Assessment of the ultrastructural and proliferative properties of human embryonic stem cell-derived cardiomyocytes. *Am. J. Physiol. Heart Circ. Physiol.* **285**, H2355–H2363 (2003).
- Laflamme, M.A. *et al.* Formation of human myocardium in the rat heart from human embryonic stem cells. *Am. J. Pathol.* **167**, 663–671 (2005).
- Kehat, I. *et al.* Electromechanical integration of cardiomyocytes derived from human embryonic stem cells. *Nat. Biotechnol.* **22**, 1282–1289 (2004).

15. Xue, T. *et al.* Functional integration of electrically active cardiac derivatives from genetically engineered human embryonic stem cells with quiescent recipient ventricular cardiomyocytes: insights into the development of cell-based pacemakers. *Circulation* **111**, 11–20 (2005).
16. Leobon, B. *et al.* Myoblasts transplanted into rat infarcted myocardium are functionally isolated from their host. *Proc. Natl. Acad. Sci. USA* **100**, 7808–7811 (2003).
17. Rubart, M., Soonpaa, M.H., Nakajima, H. & Field, L.J. Spontaneous and evoked intracellular calcium transients in donor-derived myocytes following intracardiac myoblast transplantation. *J. Clin. Invest.* **114**, 775–783 (2004).
18. Weier, H.U. *et al.* Two-color hybridization with high complexity chromosome-specific probes and a degenerate alpha satellite probe DNA allows unambiguous discrimination between symmetrical and asymmetrical translocations. *Chromosoma* **100**, 371–376 (1991).
19. Shi, Y., Evans, J.E. & Rock, K.L. Molecular identification of a danger signal that alerts the immune system to dying cells. *Nature* **425**, 516–521 (2003).
20. Zvibel, I., Smets, F. & Soriano, H. Anokis: roadblock to cell transplantation? *Cell Transplant.* **11**, 621–630 (2002).
21. Cao, G. *et al.* In vivo delivery of a Bcl-xL fusion protein containing the TAT protein transduction domain protects against ischemic brain injury and neuronal apoptosis. *J. Neurosci.* **22**, 5423–5431 (2002).
22. Baines, C.P. *et al.* Loss of cyclophilin D reveals a critical role for mitochondrial permeability transition in cell death. *Nature* **434**, 658–662 (2005).
23. Nakagawa, T. *et al.* Cyclophilin D-dependent mitochondrial permeability transition regulates some necrotic but not apoptotic cell death. *Nature* **434**, 652–658 (2005).
24. Ardehali, H., O'Rourke, B. & Mitochondrial, K. ATP channels in cell survival and death. *J. Mol. Cell. Cardiol.* **39**, 7–16 (2005).
25. Davis, M.E. *et al.* Local myocardial insulin-like growth factor 1 (IGF-1) delivery with biotinylated peptide nanofibers improves cell therapy for myocardial infarction. *Proc. Natl. Acad. Sci. USA* **103**, 8155–8160 (2006).
26. Montolio, M., Tellez, N., Biarnes, M., Soler, J. & Montanya, E. Short-term culture with the caspase inhibitor z-VAD.fmk reduces beta cell apoptosis in transplanted islets and improves the metabolic outcome of the graft. *Cell Transplant.* **14**, 59–65 (2005).
27. Zhang, M. *et al.* Cardiomyocyte grafting for cardiac repair: graft cell death and anti-death strategies. *J. Mol. Cell. Cardiol.* **33**, 907–921 (2001).
28. Zuppinger, C., Eppenberger-Eberhardt, M. & Eppenberger, H.M. N-Cadherin: structure, function and importance in the formation of new intercalated disc-like cell contacts in cardiomyocytes. *Heart Fail. Rev.* **5**, 251–257 (2000).
29. Nussbaum, J. *et al.* Transplantation of undifferentiated murine embryonic stem cells in the heart: teratoma formation and immune response. *FASEB J.* **21**, 1345–1357 (2007).
30. Swijnenburg, R.J. *et al.* Embryonic stem cell immunogenicity increases upon differentiation after transplantation into ischemic myocardium. *Circulation* **112**, 1166–1172 (2005).
31. Contreras, J.L. *et al.* Cytoprotection of pancreatic islets before and early after transplantation using gene therapy. *Kidney Int.* **61**, 79–84 (2002).
32. Nakano, M. *et al.* Caspase-3 inhibitor prevents apoptosis of human islets immediately after isolation and improves islet graft function. *Pancreas* **29**, 104–109 (2004).
33. Schierle, G.S. *et al.* Caspase inhibition reduces apoptosis and increases survival of nigral transplants. *Nat. Med.* **5**, 97–100 (1999).
34. Emgard, M. *et al.* Both apoptosis and necrosis occur early after intracerebral grafting of ventral mesencephalic tissue: a role for protease activation. *J. Neurochem.* **86**, 1223–1232 (2003).
35. Guerette, B. *et al.* Prevention by anti-LFA-1 of acute myoblast death following transplantation. *J. Immunol.* **159**, 2522–2531 (1997).
36. Skuk, D., Caron, N.J., Goulet, M., Roy, B. & Tremblay, J.P. Resetting the problem of cell death following muscle-derived cell transplantation: detection, dynamics and mechanisms. *J. Neuropathol. Exp. Neurol.* **62**, 951–967 (2003).
37. Gneocchi, M. *et al.* Paracrine action accounts for marked protection of ischemic heart by Akt-modified mesenchymal stem cells. *Nat. Med.* **11**, 367–368 (2005).
38. Gneocchi, M. *et al.* Evidence supporting paracrine hypothesis for Akt-modified mesenchymal stem cell-mediated cardiac protection and functional improvement. *FASEB J.* **20**, 661–669 (2006).
39. Ebelt, H. *et al.* Cellular cardiomyoplasty: improvement of left ventricular function correlates with the release of cardioactive cytokines. *Stem Cells* **25**, 236–244 (2007).
40. Kinnaird, T. *et al.* Marrow-derived stromal cells express genes encoding a broad spectrum of arteriogenic cytokines and promote in vitro and in vivo arteriogenesis through paracrine mechanisms. *Circ. Res.* **94**, 678–685 (2004).
41. Laflamme, M.A., Zbinden, S., Epstein, S.E. & Murry, C.E. Cell-based cardiac repair: pathophysiologic mechanisms. *Annu. Rev. Pathol. Mech. Dis.* **2**, 307–339 (2007).
42. Rubart, M. *et al.* Physiological coupling of donor and host cardiomyocytes after cellular transplantation. *Circ. Res.* **92**, 1217–1224 (2003).
43. Tallini, Y.N. *et al.* Imaging cellular signals in the heart in vivo: cardiac expression of the high-signal Ca<sup>2+</sup> indicator GCaMP2. *Proc. Natl. Acad. Sci. USA* **103**, 4753–4758 (2006).
44. Smith, J.C., Price, B.M., Van Nimmen, K. & Huylebroeck, D. Identification of a potent *Xenopus* mesoderm-inducing factor as a homologue of activin A. *Nature* **345**, 729–731 (1990).
45. Nakajima, Y., Yamagishi, T., Ando, K. & Nakamura, H. Significance of bone morphogenetic protein-4 function in the initial myofibrillogenesis of chick cardiogenesis. *Dev. Biol.* **245**, 291–303 (2002).
46. Ladd, A.N., Yatskevych, T.A. & Antin, P.B. Regulation of avian cardiac myogenesis by activin/TGFbeta and bone morphogenetic proteins. *Dev. Biol.* **204**, 407–419 (1998).
47. Sugi, Y. & Lough, J. Activin-A and FGF-2 mimic the inductive effects of anterior endoderm on terminal cardiac myogenesis in vitro. *Dev. Biol.* **168**, 567–574 (1995).
48. Lough, J. *et al.* Combined BMP-2 and FGF-4, but neither factor alone, induces cardiogenesis in non-precardiac embryonic mesoderm. *Dev. Biol.* **178**, 198–202 (1996).
49. Barron, M., Gao, M. & Lough, J. Requirement for BMP and FGF signaling during cardiogenic induction in non-precardiac mesoderm is specific, transient, and cooperative. *Dev. Dyn.* **218**, 383–393 (2000).
50. Xu, C., Police, S., Hassanipour, M. & Gold, J.D. Cardiac bodies: a novel culture method for enrichment of cardiomyocytes derived from human embryonic stem cells. *Stem Cells Dev.* **15**, 631–639 (2006).
51. Rao, B.M. & Zandstra, P.W. Culture development for human embryonic stem cell propagation: molecular aspects and challenges. *Curr. Opin. Biotechnol.* **16**, 568–576 (2005).
52. Zandstra, P.W. & Nagy, A. Stem cell bioengineering. *Annu. Rev. Biomed. Eng.* **3**, 275–305 (2001).
53. Beqqali, A., Kloots, J., Ward-van Oostwaard, D., Mummery, C. & Passier, R. Genome-wide transcriptional profiling of human embryonic stem cells differentiating to cardiomyocytes. *Stem Cells* **24**, 1956–1967 (2006).
54. Bauwens, C., Yin, T., Dang, S., Peerani, R. & Zandstra, P.W. Development of a perfusion fed bioreactor for embryonic stem cell-derived cardiomyocyte generation: oxygen-mediated enhancement of cardiomyocyte output. *Biotechnol. Bioeng.* **90**, 452–461 (2005).
55. Zandstra, P.W. *et al.* Scalable production of embryonic stem cell-derived cardiomyocytes. *Tissue Eng.* **9**, 767–778 (2003).
56. Xu, C., Police, S., Hassanipour, M. & Gold, J.D. Cardiac bodies: a novel culture method for enrichment of cardiomyocytes derived from human embryonic stem cells. *Stem Cells Dev.* **15**, 631–639 (2006).
57. Gold, J. *et al.* Efficient serum-free generation of cardiomyocytes from human embryonic stem cells in the absence of embryoid bodies (abstract). in *Circulation* **112** (17, Suppl. S), U62–U62 (2005).
58. Thomson, J.A. *et al.* Embryonic stem cell lines derived from human blastocysts. *Science* **282**, 1145–1147 (1998).
59. Xu, C. *et al.* Feeder-free growth of undifferentiated human embryonic stem cells. *Nat. Biotechnol.* **19**, 971–974 (2001).
60. Bialik, S. *et al.* The mitochondrial apoptotic pathway is activated by serum and glucose deprivation in cardiac myocytes. *Circ. Res.* **85**, 403–414 (1999).
61. Malhotra, R. & Brosius, F.C., III Glucose uptake and glycolysis reduce hypoxia-induced apoptosis in cultured neonatal rat cardiac myocytes. *J. Biol. Chem.* **274**, 12567–12575 (1999).
62. Shimizu, S., Konishi, A., Kodama, T. & Tsujimoto, Y. BH4 domain of antiapoptotic Bcl-2 family members closes voltage-dependent anion channel and inhibits apoptotic mitochondrial changes and cell death. *Proc. Natl. Acad. Sci. USA* **97**, 3100–3105 (2000).
63. Griffiths, E.J. & Halestrap, A.P. Protection by Cyclosporin A of ischemia/reperfusion-induced damage in isolated rat hearts. *J. Mol. Cell. Cardiol.* **25**, 1461–1469 (1993).
64. Halestrap, A.P., Connern, C.P., Griffiths, E.J. & Kerr, P.M. Cyclosporin A binding to mitochondrial cyclophilin inhibits the permeability transition pore and protects hearts from ischaemia/reperfusion injury. *Mol. Cell. Biochem.* **174**, 167–172 (1997).
65. Reiss, K. *et al.* Insulin-like growth factor-1 receptor and its ligand regulate the reentry of adult ventricular myocytes into the cell cycle. *Exp. Cell Res.* **235**, 198–209 (1997).
66. Mehrhof, F.B. *et al.* In cardiomyocyte hypoxia, insulin-like growth factor-I-induced antiapoptotic signaling requires phosphatidylinositol-3-OH-kinase-dependent and mitogen-activated protein kinase-dependent activation of the transcription factor cAMP response element-binding protein. *Circulation* **104**, 2088–2094 (2001).
67. Vanden Hoek, T., Becker, L.B., Shao, Z.H., Li, C.Q. & Schumacker, P.T. Preconditioning in cardiomyocytes protects by attenuating oxidant stress at reperfusion. *Circ. Res.* **86**, 541–548 (2000).
68. Akao, M., Ohler, A., O'Rourke, B. & Marban, E. Mitochondrial ATP-sensitive potassium channels inhibit apoptosis induced by oxidative stress in cardiac cells. *Circ. Res.* **88**, 1267–1275 (2001).
69. Akao, M. *et al.* Differential actions of cardioprotective agents on the mitochondrial death pathway. *Circ. Res.* **92**, 195–202 (2003).
70. Reinecke, H. & Murry, C.E. Cell grafting for cardiac repair. *Methods Mol. Biol.* **219**, 97–112 (2003).
71. Murry, C.E. *et al.* Hematopoietic stem cells do not transdifferentiate into cardiac myocytes in myocardial infarcts. *Nature* **428**, 664–668 (2004).
72. Minami, E., Laflamme, M.A., Saffitz, J.E. & Murry, C.E. Extracardiac progenitor cells repopulate most major cell types in the transplanted human heart. *Circulation* **112**, 2951–2958 (2005).
73. Nicklas, J.A. & Buel, E. Development of an Alu-based, real-time PCR method for quantitation of human DNA in forensic samples. *J. Forensic Sci.* **48**, 936–944 (2003).
74. Sambrook, J., Fritsch, E.F. & Maniatis, T. Appendix C: Properties of nucleic acids. in *Molecular Cloning, A Laboratory Manual* (Cold Spring Harbor Laboratory, Cold Spring Harbor, New York, USA, 1989).